Krüppel-like factor 6 regulates mitochondrial function in the kidney

Sandeep K. Mallipattu,[1] Sylvia J. Horne,[1] Vivette D'Agati,[2] Goutham Narla,[3] Ruijie Liu,[4] Michael A. Frohman,[5] Kathleen Dickman,[5] Edward Y. Chen,[6] Avi Ma'ayan,[6] Agnieszka B. Bialkowska,[7] Amr M. Ghaleb,[7] Mandayam O. Nandan,[7] Mukesh K. Jain,[8] Ilse Daehn,[4] Peter Y. Chuang,[4] Vincent W. Yang,[7] and John C. He[4,6,9]

[1]Division of Nephrology, Department of Medicine, Stony Brook University, Stony Brook, New York, USA. [2]Department of Pathology, Columbia University, New York, New York, USA. [3]Institute for Transformative Molecular Medicine, Case Western Reserve University, Cleveland, Ohio, USA. [4]Division of Nephrology, Department of Medicine, Mount Sinai School of Medicine, New York, New York, USA. [5]Department of Pharmacology, Stony Brook University, Stony Brook, New York, USA. [6]Department of Pharmacology and Systems Therapeutics, Mount Sinai School of Medicine, New York, New York, USA. [7]Department of Medicine, Stony Brook University, Stony Brook, New York, USA. [8]Department of Medicine, Case Cardiovascular Institute Research Institute, Case Western Reserve University, Cleveland, Ohio, USA. [9]Renal Section, James J. Peters VA Medical Center, New York, New York, USA.

Maintenance of mitochondrial structure and function is critical for preventing podocyte apoptosis and eventual glomerulosclerosis in the kidney; however, the transcription factors that regulate mitochondrial function in podocyte injury remain to be identified. Here, we identified Krüppel-like factor 6 (KLF6), a zinc finger domain transcription factor, as an essential regulator of mitochondrial function in podocyte apoptosis. We observed that podocyte-specific deletion of *Klf6* increased the susceptibility of a resistant mouse strain to adriamycin-induced (ADR-induced) focal segmental glomerulosclerosis (FSGS). KLF6 expression was induced early in response to ADR in mice and cultured human podocytes, and prevented mitochondrial dysfunction and activation of intrinsic apoptotic pathways in these podocytes. Promoter analysis and chromatin immunoprecipitation studies revealed that putative KLF6 transcriptional binding sites are present in the promoter of the mitochondrial cytochrome *c* oxidase assembly gene (*SCO2*), which is critical for preventing cytochrome *c* release and activation of the intrinsic apoptotic pathway. Additionally, *KLF6* expression was reduced in podocytes from HIV-1 transgenic mice as well as in renal biopsies from patients with HIV-associated nephropathy (HIVAN) and FSGS. Together, these findings indicate that KLF6-dependent regulation of the cytochrome *c* oxidase assembly gene is critical for maintaining mitochondrial function and preventing podocyte apoptosis.

Introduction

The glomerulus is the main filtration barrier of the human body. Podocytes, which are terminally differentiated epithelial cells in the glomerulus, play a major role in the maintenance of this renal filtration barrier. Podocyte injury is implicated in many glomerular diseases, including focal segmental glomerular sclerosis (FSGS) and HIV-associated nephropathy (HIVAN) (1). In many of these conditions, the podocyte loses specific markers of differentiation, undergoes effacement of foot processes and eventual detachment, and loses the functional capacity to maintain the glomerular filtration barrier (2).

Mitochondrial injury has been implicated in glomerular disease. Initial studies revealed altered expression of mitochondrial genes and mitochondrial dysfunction in acquired and congenital human nephrotic syndrome (3, 4). Furthermore, collapsing FSGS has been associated with mitochondrial injury with inherited mutations in genes encoding for mitochondrial function (5). Most recently, maintenance of the mitochondrial genome was shown to be critical for preventing FSGS in a murine model of adriamycin-induced (ADR-induced) podocyte injury (6). However, the mechanisms mediating the regulation of the mitochondrial injury in podocytes have yet to be characterized.

Krüppel-like factors (KLFs) are a subclass of zinc finger family of DNA-binding transcriptional regulators that are involved in a broad range of cellular processes (i.e., cell differentiation, angiogenesis, and erythropoiesis) (7). Studies have revealed a novel role of KLFs in podocyte injury (8, 9). Recently, we identified the critical role of *KLF15* in attenuating podocyte dedifferentiation in HIVAN (9). To explore the potential role of other KLFs in podocyte injury, we began by examining the expression profile of *KLF* transcripts in HIV-1–infected podocytes. We observed a significant reduction in *KLF6* expression in HIV-1–infected human podocytes and in two independent models of podocyte injury. In addition, KLF6 expression was markedly reduced in human glomerular disease. Finally, podocyte-specific loss of *Klf6* renders the kidney susceptible to mitochondrial dysfunction, resulting in activation of intrinsic apoptotic pathways and eventually glomerulosclerosis.

▶ Related Commentary: p. 968

Conflict of interest: The authors have declared that no conflict of interest exists.
Submitted: May 14, 2014; **Accepted:** December 9, 2014.
Reference information: *J Clin Invest*. 2015;125(3):1347–1361. doi:10.1172/JCI77084.

Results

KLF6 expression is reduced in HIV-1 transgenic mice. Since we recently identified the critical role of *KLF15* in attenuating podocyte dedifferentiation in HIV-1–infected podocytes, we exam-

Table 1. Quantification of histologic and ultrastructural changes

	% Segmental global GS[A]	Podocyte hypertrophy (0–3+)[B]	Podocyte hyperplasia (0–3+)[A]	Podocyte MV transformation (0–3+)[B]	% Podocyte FP effacement[B]	% IFTA/ inflammation[A]	% Tubular casts/ cystic dil[A]	Tubular degen. and regen. change (0–3+)[A]
Cre^{+} *Klf6*$^{+/+}$	0.0	–	0.0	–	–	0.0	0.0	0.0
Cre^{+} *Klf6*$^{+/+}$ + ADR	0.0	0.0	0.0	0.0	5%–10%	0.0	0.0	0.0
Cre^{+} *Klf6*$^{fl/fl}$	0.0	–	0.0	–	–	0.0	0.0	0.0
Cre^{+} *Klf6*$^{fl/fl}$ + ADR	11.0 ± 2.1	3.0 ± 0.0	1.0 ± 0.0	2.0 ± 0.0	80%–90%	1.3 ± 0.7	4.3 ± 0.7	0.7 ± 0.3

[A]Light microscopy (30 glomeruli per mouse; n = 6 mice per group). [B]Electron microscopy (n = 4 mice). All data are expressed as mean ± SEM. deg., degenerative; dil,dilatation; FP, foot process; GS, glomerulosclerosis; IFTA, interstitial fibrosis and tubular atrophy; MV, microvillous transformation; regen., regenerative.

ined the level of other KLFs in human HIVAN by measuring the expression profile of *KLFs* known to be expressed in epithelial cells (Figure 1A). In comparison to WT human podocytes, *KLF6* expression was significantly reduced in HIV-1–infected podocytes (Figure 1A, inset). We confirmed that KLF6 expression was reduced in HIV-1 transgenic (Tg26) mice as compared with WT mice (FVB/N background) (Figure 1, B and C). These findings suggest that a loss of *KLF6* may play a critical role in the podocyte injury observed in HIVAN.

Podocyte-specific loss of Klf6 increases susceptibility to ADR-induced nephropathy. To assess whether the loss of *Klf6* in podocytes results in podocyte injury and subsequent glomerulosclerosis, *Klf6* was specifically knocked down in podocytes using the Cre-loxP recombination system. *Podocin-Cre* mice (C57BL/6) were crossed with *Klf6*$^{fl/fl}$ (C57BL/6) to generate *Podocin-Cre Klf6*$^{fl/fl}$ mice (F_2). Primary culture of podocytes isolated from *Podocin-Cre Klf6*$^{+/+}$ mice and *Podocin-Cre Klf6*$^{fl/fl}$ mice revealed a significant reduction in *Klf6* mRNA and protein expression (Figure 2, A and B). These findings were confirmed with colocalization of KLF6 with WT1, a known podocyte marker (Figure 2C). All mice were viable and fertile. *Podocin-Cre Klf6*$^{fl/fl}$ mice exhibited a 3.5-fold increase in albuminuria as compared with *Podocin-Cre Klf6*$^{+/+}$ mice (Supplemental Figure 1A; supplemental material available online with this article; doi:10.1172/JCI77084DS1), but no overt histological evidence of glomerulosclerosis or tubulointerstitial disease was observed (Supplemental Figure 1B).

Prior studies have demonstrated that C57BL/6 mice are resistant to ADR-induced FSGS, unless they harbor mutations that are critical to the maintenance of the mitochondrial genome (6, 10). However, transcription factors regulating this process have yet to be identified. Therefore, we used the ADR model specifically on a resistant C57BL/6 background to determine whether the loss of *Klf6* increased the susceptibility to podocyte injury, leading to FSGS. ADR-treated *Podocin-Cre Klf6*$^{fl/fl}$ mice exhibited a significant increase in albuminuria (Figure 3A), podocyte hyperplasia, segmental glomerulosclerosis, interstitial inflammation, and tubular casts with cystic dilatation as compared with ADR-treated *Podocin-Cre Klf6*$^{+/+}$ mice (Figure 3B). In addition, electron microscopy revealed significant podocyte foot process effacement, podocyte hypertrophy, and microvillus transformation in the ADR-treated *Podocin-Cre Klf6*$^{fl/fl}$ mice as compared with the ADR-treated *Podocin-Cre Klf6*$^{+/+}$ mice (Figure 4). The quantification of these morphological changes observed by light and electron microscopy is shown in Table 1. Podocyte injury was further confirmed with a loss of key podocyte differentiation markers, *Nephrin* and *Podocin*, in the ADR-treated *Podocin-Cre Klf6*$^{fl/fl}$ mice as compared with all other groups (Supplemental Figure 2, A and B). Taken together, these findings highlight that *Klf6* is required to prevent podocyte injury and eventual glomerulosclerosis in the setting of ADR treatment.

Podocyte-specific Klf6-knockout mice exhibit mitochondrial injury with ADR treatment. Prior studies have suggested that ADR-induced mitochondrial damage plays a major role in cellular injury in several other tissues (11–14). Similarly, ultrastructural examination of the podocyte cell bodies revealed dysmorphic mitochondria in the ADR-treated *Podocin-Cre Klf6*$^{fl/fl}$ mice as compared with ADR-treated *Podocin-Cre Klf6*$^{+/+}$ mice (Figure 5, A and B). Promoter analysis was subsequently performed to assess whether transcriptional binding sites for KLF6 exist in the proximity of genes involved in mitochondrial function. TRANSFAC (15) promoter analysis revealed eight potential KLF6 binding sites in the cytochrome *c* oxidase assembly gene (*SCO2*) (Table 2). We initially confirmed that putative binding sites for KLF6 are present along the promoter region of *SCO2* using ChIP followed by quantitative RT-PCR in cultured human podocytes (Figure 6A). Podocytes from ADR-treated *Podocin-Cre Klf6*$^{fl/fl}$ mice exhibited a significant reduction in *Sco2* mRNA expression as compared with podocytes from ADR-treated *Podocin-Cre Klf6*$^{+/+}$ mice (Figure 6B). Similarly, SCO2 expression was significantly

Table 2. Predicted KLF6 binding sites

Gene symbol	Description	Binding sites
SCO2	Cytochrome *c* oxidase (COX) assembly gene	8
PCSK6	Proprotein convertase subtilisin/kexin type 6	5
SHARPIN	SHANK-associated RH domain interactor	4
CHODL	Chondrolectin	3
LEMD2	LEM domain containing 2	2
ARFRP1	ADP-ribosylation factor-related protein 1	2
WDR46	Chromosome 6 open reading frame 11	2
KCNIP4	Kv channel interacting protein 4	2
WDR38	WD repeat-containing protein 38	2
GPRC5C	G protein-coupled receptor, family C, group 5, member C	2

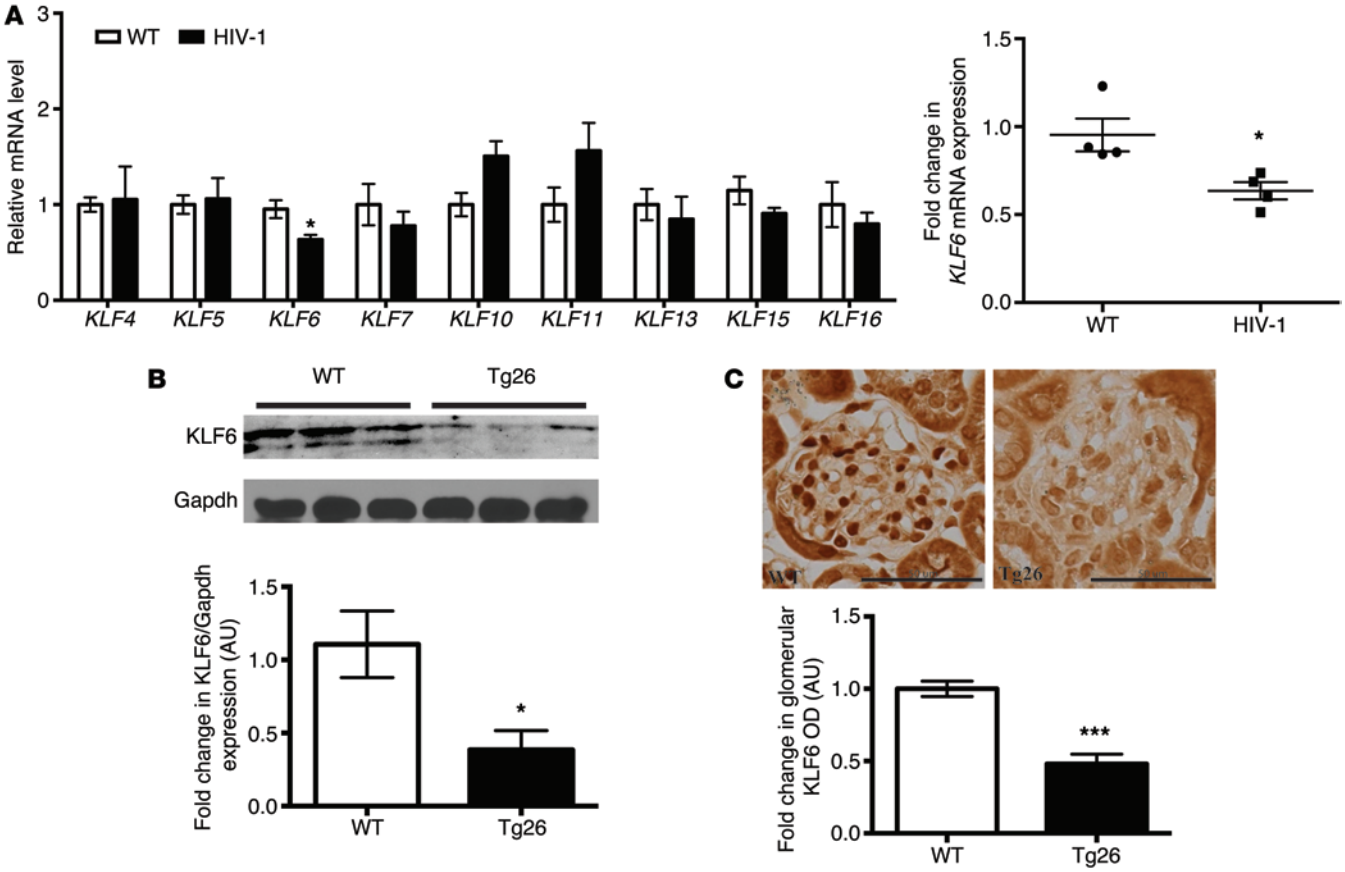

Figure 1. Strong association between KLF6 and the glomerulosclerosis was observed in HIVAN. (**A**) mRNA levels of *KLF*s, previously shown to be expressed in epithelial cells, were measured in differentiated WT and HIV-1–infected human podocytes in culture. Real-time PCR, using primers for *KLF4*, *KLF5*, *KLF6*, *KLF7*, *KLF10*, *KLF11*, *KLF13*, *KLF15*, and *KLF16*, was performed using RNA isolated from WT and HIV-1–infected human podocytes. Inset: Relative mRNA expression for *KLF6* ($n = 4$). Mann-Whitney *U* test, $^*P < 0.05$. (**B**) Age- and sex-matched 6-week-old HIV-1 transgenic mice (Tg26) and WT mice on the FVB/N background were used to assess KLF6 expression in the glomeruli. Western blot analysis was performed on the glomerular lysates from WT and Tg26 mice for KLF6 and GAPDH. A representative blot of six independent experiments is shown in the top panel. The bottom panel shows the quantification of KLF6 by densitometry ($n = 6$). Mann-Whitney *U* test, $^*P < 0.05$. (**C**) The top panel shows representative images of immunohistochemistry for KLF6 in kidney sections from WT and Tg26 mice ($n = 8$ mice) (original magnification, ×20). Bottom panel: 30 glomeruli were selected in each mouse, and the intensity of KLF6 expression was quantified in the glomerular region ($n = 8$ mice). Unpaired *t* test, $^{***}P < 0.001$.

reduced in ADR-treated *Podocin-Cre Klf6*$^{fl/fl}$ mice as compared with all other groups (Figure 6C). SCO2 is a mitochondrial membrane–bound metallochaperone critical to the transport of copper atoms to cytochrome *c* oxidase (COX) subunits I and II; therefore, it is essential for the assembly of the catalytic core of the COX complex (16, 17). Using antibodies specific for COX subunit II (MT-CO2), we observed that MT-CO2 is expressed in the glomerular compartment (Figure 6D). Furthermore, we determined that MT-CO2 expression was significantly reduced in ADR-treated *Podocin-Cre Klf6*$^{fl/fl}$ mice as compared with ADR-treated *Podocin-Cre Klf6*$^{+/+}$ mice (Figure 6D).

Because our results suggest that KLF6 may play a critical role in the regulation of mitochondrial gene expression, we sought to determine the level of expression of other transcripts involved in mitochondrial function. First, podocytes were isolated from *Podocin-Cre Klf6*$^{fl/fl}$ and *Podocin-Cre Klf6*$^{+/+}$ mice and treated with ADR in primary culture for 12 hours. RNA transcripts involved in mitochondrial replication and transcription (nuclear respiratory factor 1 [*Nrf1*], polymerase mitochondrial [*Polrmt*], transcription factor A mitochondrial [*Tfam*]) and mitochondrial function (*mt-Co2*, COX subunit 8A [*Cox8a*], mitochondrial inner membrane protein [*Mpv17*]) were significantly reduced in ADR-treated podocytes isolated from *Podocin-Cre Klf6*$^{fl/fl}$ mice as compared with ADR-treated podocytes isolated from *Podocin-Cre Klf6*$^{+/+}$ mice (Supplemental Figure 3, A and B). Taken together, these data suggest that *Klf6* is required for the maintenance of mitochondrial function and preventing podocyte injury in the setting of ADR exposure.

KLF6 is required to protect podocytes from ADR-induced mitochondrial injury. In order to assess *Klf6* expression pattern and activity in podocytes exposed to ADR, podocytes isolated from WT mice were treated with and without ADR in primary culture for 12 hours. We observed a significant increase in *Klf6* mRNA expression in ADR-treated podocytes as compared with untreated podocytes in culture (Figure 7A). Similarly, a significant increase in KLF6 expression was observed in ADR-treated WT mice as compared with untreated mice (Figure 7B). Additionally, KLF6 protein expression was significantly increased within 6 hours of ADR exposure in cultured human podocytes (Figure 7C).

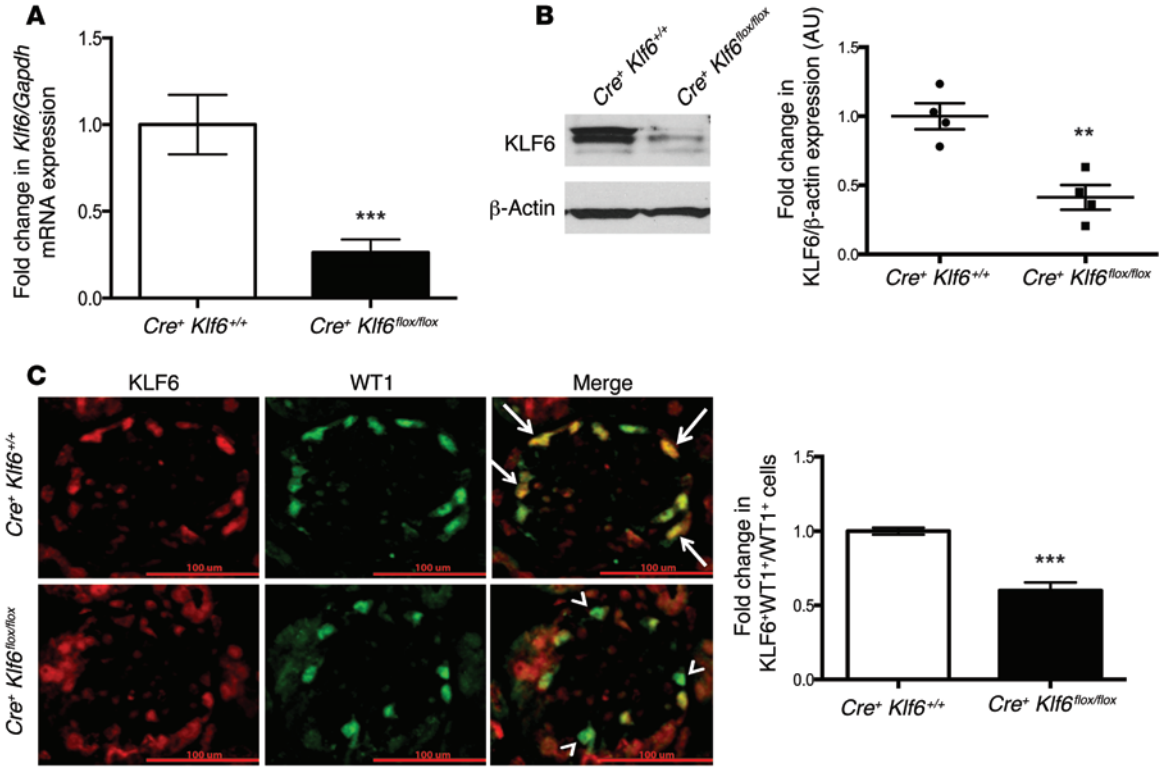

Figure 2. Podocyte-specific knockdown of *Klf6* in *Podocin-Cre Klf6$^{fl/fl}$* mice was confirmed. (**A**) Primary podocytes were isolated from 10-week-old *Podocin-Cre Klf6$^{fl/fl}$* and *Podocin-Cre Klf6$^{+/+}$* mice and cultured at 37°C for 1 week. RNA was extracted, and real-time PCR was performed for *Klf6* mRNA expression (n = 6). Mann-Whitney U test, $^{***}P < 0.001$. (**B**) Protein was also extracted, and Western blot analysis was performed for KLF6. A representative blot of four independent experiments is shown in the left panel (KLF6 and β-actin are from the same samples on the same blot, with β-actin being developed after KLF6). The right panel shows the quantification of KLF6 by densitometry (n = 4). Mann-Whitney U test, $^{**}P < 0.01$. (**C**) Immunofluorescence staining for KLF6 and WT1 was performed in 10-week-old *Podocin-Cre Klf6$^{fl/fl}$* and *Podocin-Cre Klf6$^{+/+}$* mice. Representative images from six mice in each group are shown in the left panel (original magnification, ×20). Arrows show colocalization of KLF6 and WT1. Arrowheads show a lack of colocalization. Right panel: 30 glomeruli were selected in each mouse, and quantification of KLF6 staining in the podocytes was determined by the ratio of KLF6$^+$ and WT1$^+$ cells to WT1$^+$ cells (n = 6 mice). Unpaired t test, $^{***}P < 0.001$.

Immunostaining for KLF6 with and without ADR treatment at 12 hours confirmed the increase in KLF6 expression (Figure 7D), suggesting that *KLF6* is an early inducible gene. Since KLF6 activity is initially increased with ADR exposure in podocytes and the loss of *Klf6* in podocytes increased the susceptibility to ADR-induced podocyte injury, we hypothesized that *KLF6* is required to protect podocytes from ADR-induced mitochondrial injury. To evaluate this, we first generated human podocytes with stable knockdown for *KLF6* (Supplemental Figure 4A). As compared with WT human podocytes, the loss of *KLF6* resulted in a decrease in mitochondrial membrane potential (Figure 8A). Since *SCO2* was shown to be a transcriptional target of KLF6, we measured SCO2 expression in this model. SCO2 expression was significantly reduced in shRNA-*KLF6* podocytes treated with or without ADR (Figure 8B). Furthermore, shRNA-*KLF6* podocytes exhibited a significant reduction in ATP activity and oxygen consumption rate with ADR treatment (Figure 8, C and D). In addition, mitochondrial biomass was not significantly different between the groups (Supplemental Figure 4B), suggesting that the loss in mitochondrial function was not a result of reduced mitochondrial number. We also observed that the shRNA-*KLF6* podocytes exhibited an increase in mitochondrial fragmentation with ADR treatment (Figure 8E). Additionally, merely the knockdown of KLF6 shifted the morphology of the mitochondria from a tubular pattern to an intermediate pattern (Figure 8E). To assess whether the reintroduction of *KLF6* can rescue the cells from mitochondrial injury, LentiORF-*KLF6* was transiently transfected in *EVshRNA-KLF6* human podocytes (Supplemental Figure 4C). Subsequent restoration of *KLF6* in shRNA-*KLF6* podocytes prevented mitochondrial fragmentation and preserved the tubular structural pattern of the mitochondria (Figure 8F). Combined, these findings suggest that *KLF6* is an early inducible injury response gene, critical to the maintenance of mitochondrial function upon injury.

KLF6 mediates apoptosis in the setting of ADR treatment. ADR has been previously shown to activate intrinsic apoptotic pathways in other models of tissue injury (18–20); we showed that a loss of *KLF6* increased the susceptibility to ADR-induced mitochondrial injury. Therefore, we hypothesized that a loss of *KLF6* would result in the activation of intrinsic apoptotic pathways with ADR treatment. Initially, we observed that shRNA-*KLF6* podocytes exhibited a significant increase in apoptotic bodies with ADR treatment (Figure 9A). This increase in apoptotic cells was quantified using flow cytometry with annexin V and propidium iodide labeling (Figure 9B). Furthermore, we demonstrated that release

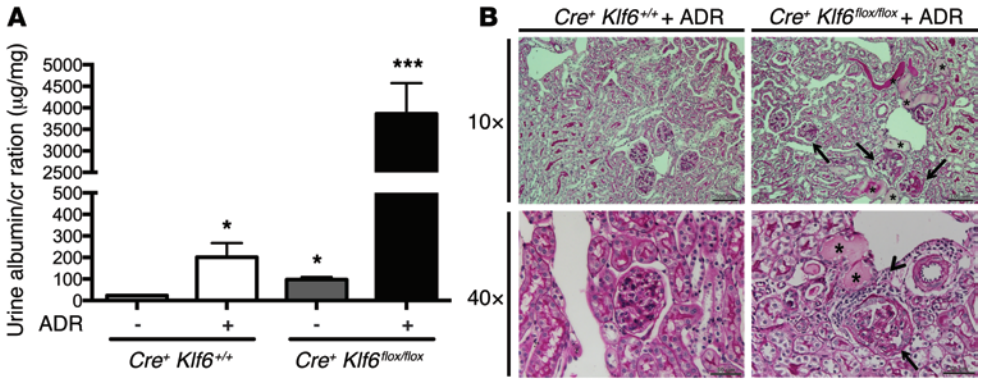

Figure 3. ADR-treated *Podocin-Cre Klf6*$^{fl/fl}$ mice exhibit a significant increase in albuminuria with glomerulosclerosis and tubulointerstitial injury. *Podocin-Cre Klf6*$^{fl/fl}$ and *Podocin-Cre Klf6*$^{+/+}$ mice were treated with ADR at 12 weeks of age. Urine was collected weekly, mice were sacrificed, and renal cortex was fixed for histology 5 weeks after ADR treatment. (**A**) Albuminuria (urine albumin/creatinine [cr]) was measured (n = 10). Kruskal-Wallis test with Dunn's post-hoc test, $^*P < 0.05$ as compared with untreated *Podocin-Cre Klf6*$^{+/+}$ mice, $^{***}P < 0.001$ as compared with all groups. (**B**) PAS was used to evaluate glomerular or tubulointerstitial changes (top panel: original magnification, ×10; bottom panel: original magnification, ×40). Representative images from six mice in each group are shown. Arrows show sclerotic glomeruli. Arrowheads show interstitial inflammation. Asterisks within images show tubular casts and dilatation.

of cytochrome *c* was substantially increased in shRNA-*KLF6* podocytes exposed to ADR (Figure 9C). In addition, we observed a significant increase in cleaved caspase-9 and cleaved caspase-3 levels with a decrease in procaspase-3 expression in shRNA-*KLF6* podocytes treated with ADR (Figure 9D).

To assess whether the preservation of KLF6 prevents the activation of caspases, we first generated human podocytes with stable overexpression of *KLF6* (LentiORF-*KLF6*) (Figure 9E). The overexpression of KLF6 in podocytes contributed to a significant increase in SCO2 and procaspase-3 expression, with a reduction in cleaved caspase-3 levels, in the setting of ADR treatment (Figure 9E). We observed a reduction, albeit not statistically significant, in cleaved caspase-9 levels in LentiORF-*KLF6* as compared with LentiORF-control human podocytes. Combined, these data suggest that *KLF6* prevents the ADR-induced activation of the intrinsic apoptotic pathway.

SCO2, a downstream target of KLF6, is critical to the prevention of mitochondrial injury. To confirm that *SCO2*, a critical downstream target of KLF6, is reduced in other models of podocyte injury, we used the HIV-1 transgenic mice model. We initially observed a decrease in KLF6 expression in HIV-1–infected human podocytes and in HIV-1 transgenic (Tg26) mice. We also demonstrated that SCO2 expression was reduced in the shRNA-*KLF6* podocytes and in the glomeruli of *Podocin-Cre Klf6*$^{fl/fl}$ mice (Figure 6C and Figure 8B). Similarly, *Sco2* mRNA expression was reduced in primary podocytes isolated from Tg26 mice as compared with WT mice, with both groups on the FVB/N background (Figure 10A). These findings were confirmed by immunostaining for SCO2 in glomeruli from WT and Tg26 mice (FVB/N background) (Figure 10B). These data suggest that KLF6 is required for the maintenance of SCO2 in the setting of injury.

Since KLF6 binding sites are present in the promoter region of *SCO2* and the loss of KLF6 activates the intrinsic apoptotic pathway under stress, we suspected that SCO2 is a downstream target of KLF6 and is essential to mitochondrial stability and preventing the release of cytochrome *c*. To ascertain this, we first generated human podocytes with transient knockdown of *SCO2* (Figure 10C). The transient knockdown of *SCO2* resulted in increased cleaved caspase-9 levels (Figure 10C). As compared with WT human podocytes, shRNA-*SCO2* podocytes exhibited a substantial release in cytochrome *c* from the mitochondria, as shown by an increase in the diffuse pattern of cytochrome *c* staining (Figure 10D). Taken together, these data suggest that SCO2 is a critical downstream target of KLF6-mediated mitochondrial regulation.

KLF6 expression is reduced in human FSGS. To ascertain the role of KLF6 in human glomerulopathy, immunohistochemistry was performed on renal biopsy specimens from healthy donor nephrectomies, HIVAN, and noncollapsing idiopathic FSGS. We observed that the staining for KLF6 had a nuclear distribution in the normal podocytes and parietal epithelial cells, with a nuclear and cytosolic distribution in tubular cells (Figure 11A, healthy donor). The staining also revealed a significant decrease in KLF6 expression in HIVAN and noncollapsing FSGS as compared with healthy donor nephrectomies (Figure 11A). Since KLF6 is a ubiquitous transcription factor expressed in majority of the compartments in the kidney, colocalization using KLF6 and WT1 (a known nuclear-distributed podocyte marker) was performed to determine whether the reduction in KLF6 expression is specific to

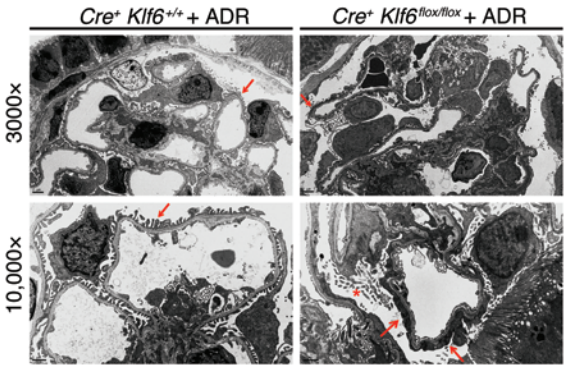

Figure 4. *Podocin-Cre Klf6*$^{fl/fl}$ mice exhibit substantial podocyte injury with ADR treatment. *Podocin-Cre Klf6*$^{fl/fl}$ and *Podocin-Cre Klf6*$^{+/+}$mice were treated with ADR at 12 weeks of age. All mice were sacrificed, and renal cortex was fixed for histology 5 weeks after ADR treatment. Electron microscopy was performed to assess ultrastructural changes in podocyte morphology (top panels: original magnification, ×3,000; bottom panels: original magnification, ×10,000). Representative images are shown from four mice in each group. Red arrows indicate the change in podocyte foot process morphology. Red asterisks show microvillus transformation.

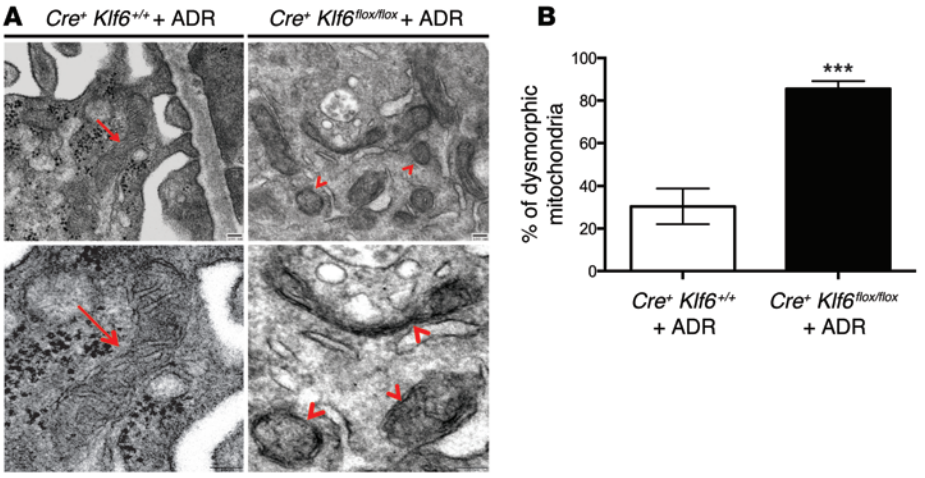

Figure 5. *Podocin-Cre Klf6*$^{fl/fl}$ mice exhibit dysmorphic mitochondria in podocytes with ADR treatment. *Podocin-Cre Klf6*$^{fl/fl}$ and *Podocin-Cre Klf6*$^{+/+}$ mice were treated with ADR at 12 weeks of age. All mice were sacrificed, and renal cortex was fixed for histology 5 weeks after ADR treatment. (**A**) Electron microscopy was performed to assess ultrastructural changes in the mitochondria of the podocyte cell body (top panels: original magnification, ×50,000; bottom panels: original magnification, ×75,000). Representative images are shown from six mice in each group. Red arrows show elongated mitochondria with preserved cristae and membrane. Red arrowheads show the loss of cristae and the loss of elongated morphology in the mitochondria. (**B**) To quantify dysmorphic mitochondria, a total of 100 mitochondrial podocytes per mouse were selected from each group to identify the percentage of mitochondria with a focal loss of visible cristae, clustering of residual cristae at the peripheral mitochondrial membrane, and length of <2 μm (n = 4 mice). Unpaired t test, ***$P < 0.001$.

the podocyte. Immunostaining revealed a significant decrease in KLF6 expression in podocytes of patients with FSGS as compared with healthy donor nephrectomies, as shown by the reduction in the number of cells with both KLF6 and WT1 staining (Figure 11B). Quantification of immunostaining in podocytes confirmed the decrease in KLF6 expression (Figure 11C). Furthermore, the specificity of the KLF6 staining was confirmed by utilizing a peptide block with the immunizing peptide (Supplemental Figure 5). Collectively, with the rest of our findings, these data suggest that KLF6 expression is reduced in human FSGS, contributing to podocyte injury observed in FSGS.

Discussion

Several studies have characterized the critical role of mitochondrial dysfunction in podocytopathy. However, transcriptional regulators mediating the effects of mitochondrial dysfunction in podocyte injury have yet to be characterized. A recent study by Papeta et al. (6) has identified that the maintenance of the mitochondrial genome is essential in preventing ADR-induced FSGS. Here, we identify that *KLF6* is a critical mediator of ADR-induced mitochondrial dysfunction in podocytes. This was demonstrated by the following: (a) podocyte-specific loss of *Klf6* resulted in ADR-induced FSGS in a resistant mouse strain (C57BL/6) and (b) shRNA-mediated *KLF6* knockdown in human podocytes resulted in mitochondrial dysfunction, as measured by reduced expression of mitochondrial transcripts, mitochondrial fragmentation, ATP levels, and oxygen consumption rate. In addition, we determined that *KLF6* is an early inducible injury response gene and it is critical for the prevention of the ADR-induced mitochondrial injury in podocytes. Furthermore, we showed that *KLF6* is required to prevent the activation of ADR-mediated intrinsic apoptotic pathway in podocytes. Finally, we confirmed that the podocyte expression of KLF6 is reduced in a murine model of HIVAN and in human HIVAN and FSGS.

Although the podocyte-specific loss of *Klf6* resulted in minimal podocyte injury at baseline, these mice developed FSGS with ADR treatment on a resistant C57BL/6 background. In combination with the early increase in KLF6 expression observed with ADR treatment, this suggests that *KLF6* is an early inducible injury response gene that may serve to protect podocytes from injury. Recently, we published that *KLF15* is a critical transcriptional regulator of podocyte differentiation (21). Furthermore, *KLF4* was found to play a critical role in regulating mitochondrial fusion proteins in vascular smooth muscle differentiation (22). In addition, paralogs of *KLF1* (specificity proteins) have been shown to transcriptionally regulate cytochrome *c* subunit genes in primary neurons (23). Future studies will focus on the potential interactions between these other *KLFs* in mediating mitochondrial function with *KLF6* in the setting of podocyte injury.

A few transcription factors have been associated with podocyte apoptosis in recent years, including FOXO4 and NF-κB (24, 25). However, none of these have been implicated in mitochondrial dysfunction leading to activation of apoptosis and eventual podocyte injury. To date, *KLF6* is, to our knowledge, the first transcription factor that is critical to the maintenance of the mitochondrial structure and function, and in preventing apoptosis in the setting of cell stress.

Analysis of the promoter region of the *COX assembly (SCO2)* gene revealed several potential binding sites for KLF6. SCO2 is an inner mitochondrial membrane metallochaperone critical to the transport of copper ions. In fact, missense mutations in *SCO2* have been found to cause fatal hypertrophic cardiomyopathy with encephalopathy (26, 27). We observed that *SCO2* is a critical downstream target of KLF6-mediated mitochondrial function, in which a loss of *SCO2* resulted in the activation of the intrinsic apoptotic pathway. In normal conditions, we hypothesize that in the early phase of ADR treatment (i.e., early cell stress), the upregulation of KLF6 results in the activation of *SCO2*, thereby abrogating mitochondrial injury and protecting the cell from injury. Nonetheless, we recognize that KLF6 may also regulate other genes involved in the activation of the intrinsic apoptotic pathway and mitochondrial injury. Although ADR has typically been observed to activate the intrinsic apoptotic pathway leading to tissue damage (19, 20), the potential crosstalk between the extrinsic and intrinsic pathway in the setting of *KLF6* depletion has to be further explored. Future studies will also need to determine the interaction between KLF6 and protein kinase, DNA-activated, catalytic peptide (PRKDC), a

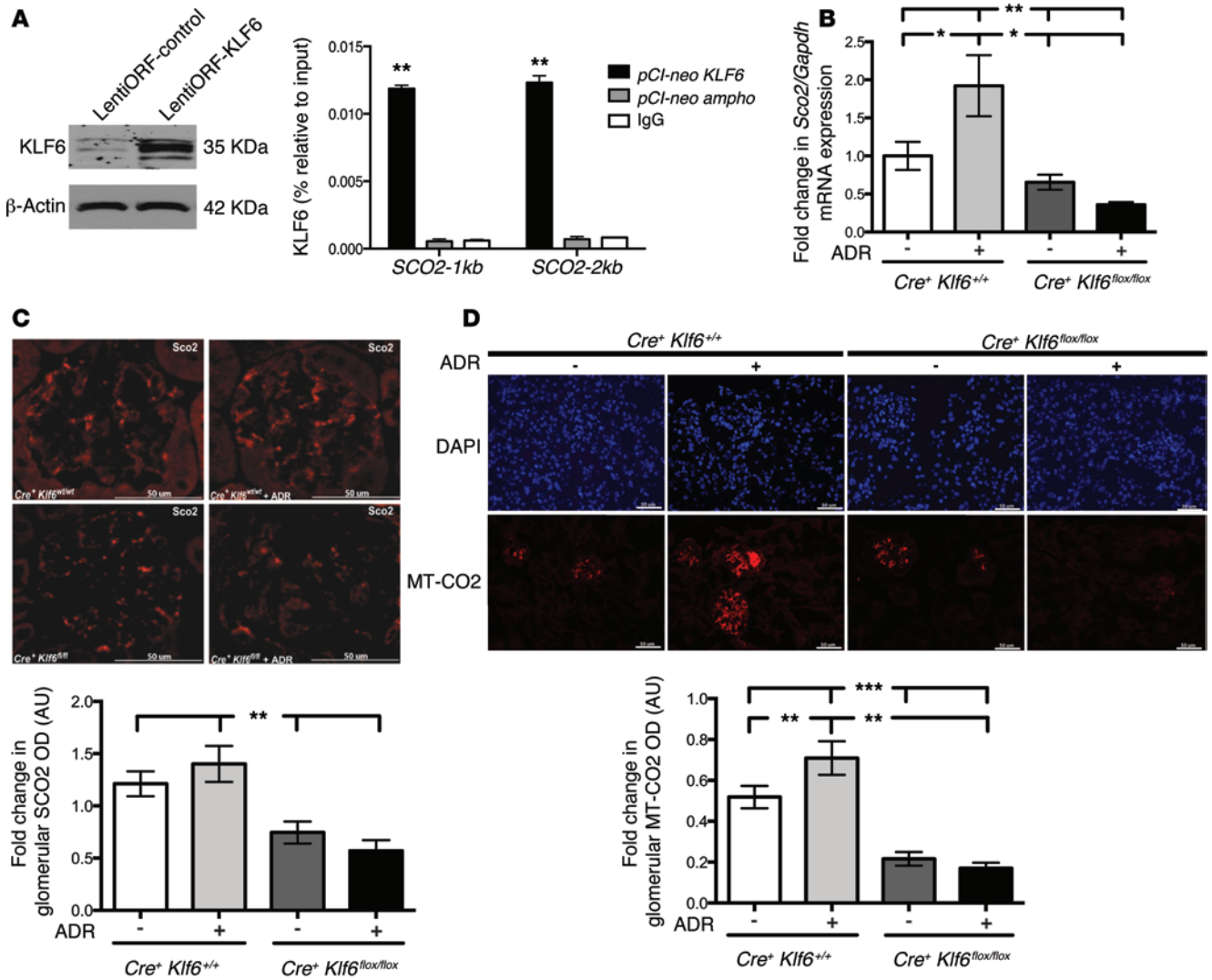

Figure 6. KLF6 binds to the promoter region of *SCO2*. To confirm that binding sites for KLF6 are present in the promoter region of *SCO2*. *KLF6* was initially overexpressed in HEK 293 cells using LentiORF transfection, and ChIP was performed. (**A**) Overexpression of KLF6 was confirmed with Western blot analysis (left panel), and the presence of putative KLF6 binding sites in the promoter of *SCO2* in HEK 293 cells is shown (right panel) (n = 4). Kruskal-Wallis test with Dunn's post-hoc test, $^{**}P < 0.01$ vs. the two other groups. (**B**) Cultured podocytes were treated with ADR for 12 hours, RNA was extracted for real-time PCR, and *Sco2* mRNA expression is shown (n = 4). Kruskal-Wallis test with Dunn's post-hoc test, $^{*}P < 0.05$, $^{**}P < 0.01$. (**C**) SCO2 expression level was also confirmed by immunofluorescence in *Podocin-Cre Klf6*$^{fl/fl}$ and *Podocin-Cre Klf6*$^{+/+}$ mice treated with and without ADR. Representative pictures of six mice in each group are shown in the top panel (original magnification, ×20). A total of 30 glomeruli per mouse were selected, and SCO2 expression was quantified in the glomerular region (n = 6) shown in the bottom panel. Kruskal-Wallis test with Dunn's post-hoc test, $^{**}P < 0.01$. (**D**) MT-CO2 levels were assessed in *Podocin-Cre Klf6*$^{fl/fl}$ and *Podocin-Cre Klf6*$^{+/+}$ mice treated with and without ADR. Representative immunofluorescence images of six mice in each group are shown in the top panel (original magnification, ×20). A total of 30 glomeruli per mouse were selected, and MT-CO2 expression was quantified in the glomerular region (n = 6) in the bottom panel. Kruskal-Wallis test with Dunn's post-hoc test, $^{**}P < 0.01$, $^{***}P < 0.001$.

nuclear DNA repair protein recently discovered to be critical to the maintenance of the mitochondrial genome in ADR-induced FSGS (6). Alternatively, KLF6 may also participate in maintaining the mitochondrial structure and function in response to DNA damage. Therefore, we expect a wide range of future studies to decipher the precise molecular mechanism mediating the interaction between KLF6 and maintenance of mitochondrial structure and function.

We also confirmed that podocyte-specific expression of KLF6 was markedly reduced in renal biopsies from patients with HIVAN and FSGS, suggesting that a loss of KLF6 expression may contribute to the podocyte injury observed in glomerular disease. Although podocyte depletion occurs in FSGS, the ratio of KLF6^{+}WT1^{+} cells to WT1^{+} cells is suggestive of reduced KLF6 expression independent of podocyte loss. In addition, our immunohistochemistry studies are suggestive of reduced KLF6 expression in the parietal epithelial cells. However, further colocalization studies with KLF6 and a known parietal epithelial cell marker need to be performed to validate our findings. Since there is a reduction in KLF6 expression with FSGS, further knockdown of *Klf6* in HIV-1 transgenic mice may not yield a significant change in an already severely diseased phenotype. Consequently, we demonstrated that the restoration of KLF6 attenuated mitochondrial injury in the setting of ADR treatment.

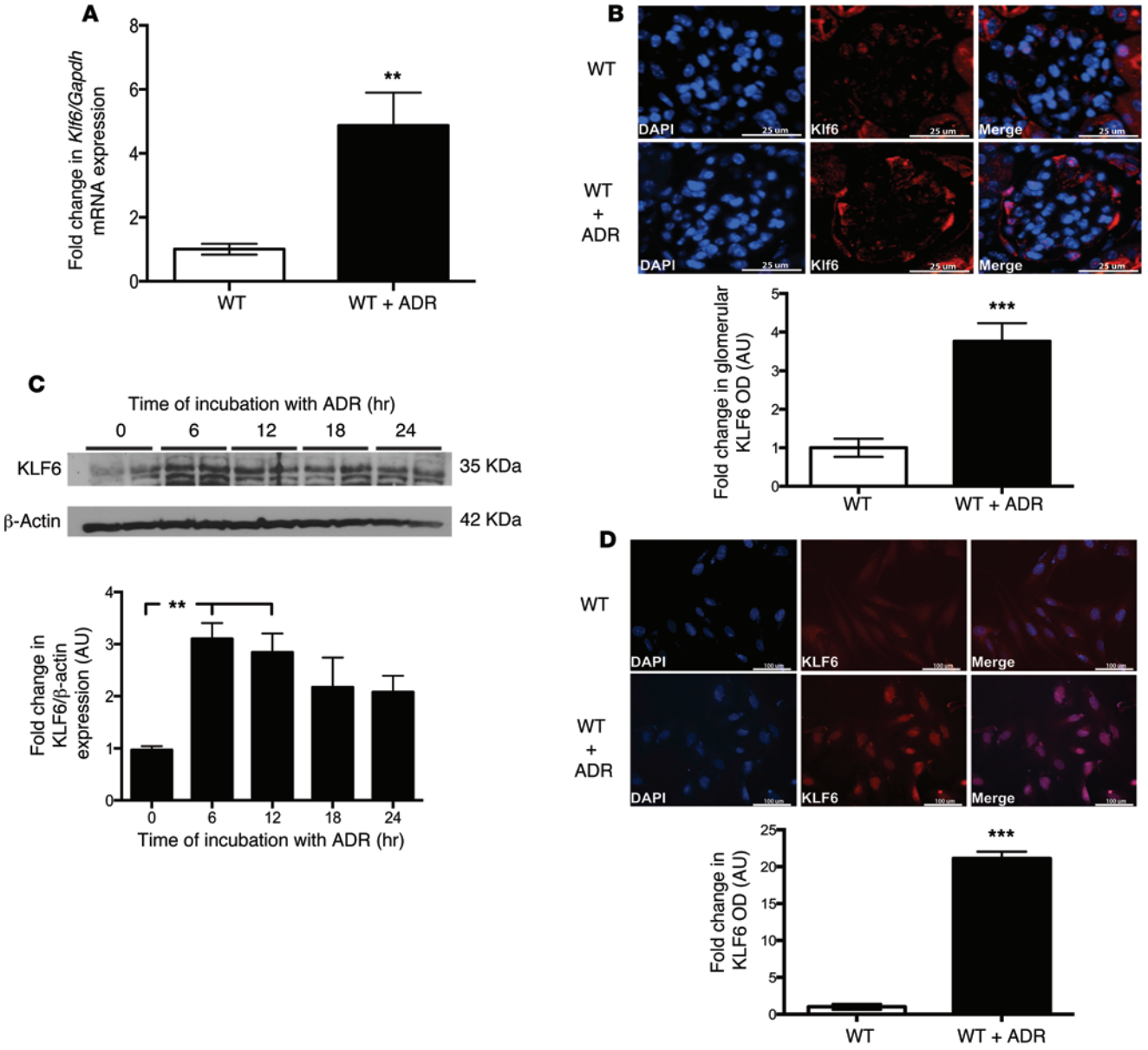

Figure 7. KLF6 expression is increased early with ADR treatment. Primary podocytes isolated from WT mice were treated with and without ADR for 12 hours. RNA was extracted, and real-time PCR was performed. (**A**) *Klf6* mRNA expression was compared between primary cultured murine podocytes treated with and without ADR ($n = 5$). Mann-Whitney *U* test, $^{**}P < 0.01$. (**B**) This was confirmed by immunofluorescence using tissue from WT mice treated with and without ADR. Representative pictures of six mice in each group are shown in the top panel (original magnification, ×20). Bottom panel: 30 glomeruli per mouse were selected, and KLF6 expression was quantified in the glomerular region ($n = 6$). Unpaired *t* test, $^{***}P < 0.001$. (**C**) Cultured human podocytes were treated with ADR for 6, 12, 18, and 24 hours. Protein was extracted, and Western blot analysis was performed for KLF6. A representative blot of three independent experiments is shown in the top panel. Densitometry analysis is shown in the bottom panel ($n = 6$). Kruskal-Wallis test with Dunn's post-hoc test, $^{**}P < 0.01$ vs. untreated cells. (**D**) Immunofluorescence staining for KLF6 with and without ADR for 12 hours is shown. Representative images of six independent experiments are shown in the top panel (original magnification, ×20, scale bar: 100 μm). In the bottom panel, the intensity of KLF6 expression was quantified ($n = 6$). Unpaired *t* test, $^{***}P < 0.001$.

However, further studies are needed to determine whether overexpression of *Klf6* protects against podocyte injury with HIV-1 transgene expression. Although, along with other investigators, we have highlighted that podocyte dedifferentiation is a hallmark in HIVAN (28, 29), recent data suggest the potential role of parietal epithelial cell proliferation in podocyte injury (30). The role of KLF6 in parietal cell proliferation remains to be explored. Nonetheless, mitochondrial injury does occur in HIV-1–infected podocytes and tubular cells (31, 32), suggesting a common final pathway in podocyte injury leading to eventual podocyte loss and glomerulosclerosis in both HIVAN and ADR nephropathy. Combined, these findings suggest that KLF6, as with ADR nephropathy, may play a critical role in protecting podocytes from injury in HIVAN.

Taken together, our results provide a potential mechanism for the transcriptional regulation of the intrinsic apoptotic pathway in podocytopathy. Our data suggest that *KLF6* is a critical injury

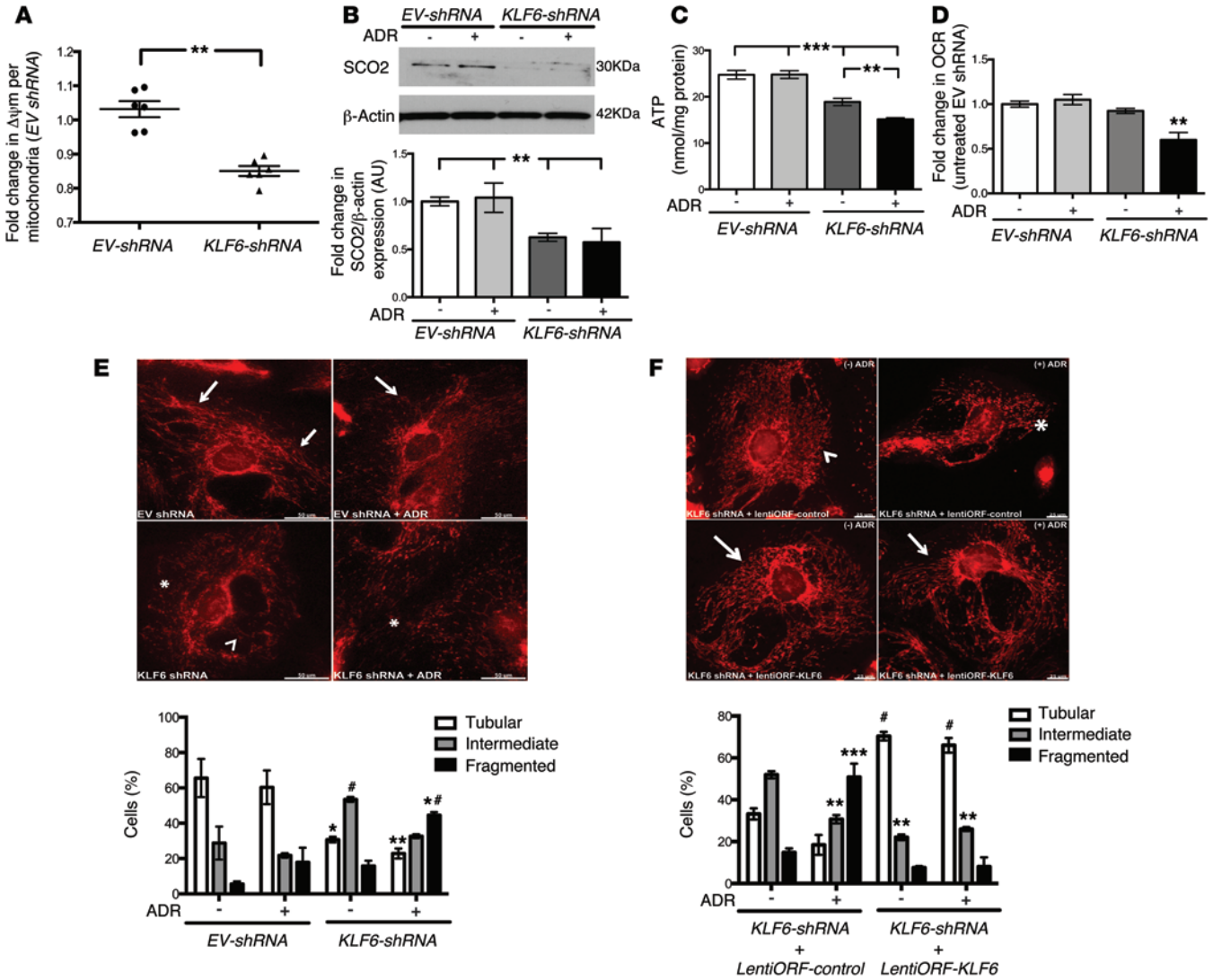

Figure 8. shRNA-mediated *KLF6* knockdown increased the susceptibility to mitochondrial injury. *EV-shRNA* and *KLF6-shRNA* human podocytes were treated with and without ADR for 24 hours. (**A**) Mitochondrial membrane potential was quantified ($n = 6$). Mann-Whitney *U* test, $^{**}P < 0.01$. (**B**) Top panel: Western blot analysis for SCO2 was performed, and representative images of six independent experiments are shown (SCO2 and β-actin are from the same samples on the same blot, with β-actin being developed after SCO2). Bottom panel: Quantification of SCO2 by densitometry ($n = 6$). Kruskal-Wallis test with Dunn's post-hoc test, $^{**}P < 0.01$. (**C**) ATP levels were quantified ($n = 8$). Kruskal-Wallis test with Dunn's post-hoc test, $^{**}P < 0.01$, $^{***}P < 0.001$. (**D**) Extracellular oxygen consumption rate (OCR) was measured and expressed as fold change relative to untreated *EV-shRNA* podocytes ($n = 6$). Kruskal-Wallis test with Dunn's post-hoc test, $^{**}P < 0.01$. (**E**) Rosamine-based MitoTracker probe was used to assess mitochondrial structure and fragmentation. Top panel: Representative images of six independent experiments (original magnification, ×20). Mitochondrial staining is indicated by tubular (arrows), intermediate (arrowheads), and fragmented (asterisks within images) pattern. Bottom panel: Scoring of mitochondrial morphology from 100 podocytes in each group ($n = 6$). Two-way ANOVA test with Tukey's post-test, $^{*}P < 0.05$ vs. tubular *EV-shRNA*, $^{**}P < 0.01$ vs. tubular *EV-shRNA*, $^{\#}P < 0.05$ vs. all intermediate groups, $^{*\#}P < 0.05$ vs. all fragmented groups. (**F**) To assess whether the reintroduction of *KLF6* can rescue the cells from mitochondrial injury, LentiORF-*KLF6* was transiently transfected in *EVshRNA-KLF6* human podocytes, and MitoTracker probe was used to assess mitochondrial fragmentation. Top panel: Representative images of three independent experiments (original magnification, ×20). Bottom panel: Scoring of mitochondrial morphology from 100 podocytes in each group ($n = 3$). Two-way ANOVA test with Tukey's post-hoc test, $^{\#}P < 0.0001$ vs. tubular *KLF6-shRNA*+LentiORF-control groups, $^{**}P < 0.01$ vs. intermediate untreated tubular *KLF6-shRNA*+LentiORF-control group; $^{***}P < 0.001$ vs. all fragmented groups.

response gene in podocytes with a strong linkage to glomerulosclerosis. Further elucidation of the mechanism by which KLF6 regulates mitochondrial structure and function may uncover potential therapeutic targets in podocytopathy.

Methods

Genotyping of Tg26 mice. Derivation of a transgenic mouse line (Tg26 mice) that bears a defective HIV-1 provirus lacking gag-pol (Tg26) has been described (33). Tg26 mice are in the FVB/N background. Mice generated from the same litter of Tg26 mice were used as controls in the studies. Genotyping by tail preparation and PCR were performed at 2 weeks of age as previously described (34).

Genotyping of Podocin-Cre Klf6$^{fl/fl}$ mice. Mice with *Klf6*-targeting vector (C57BL/6) were generated using the targeting strategy as previously described (35). *Klf6$^{fl/fl}$* mice (C57BL/6) were crossed with mice expressing *Cre* recombinase (cre) under the control of

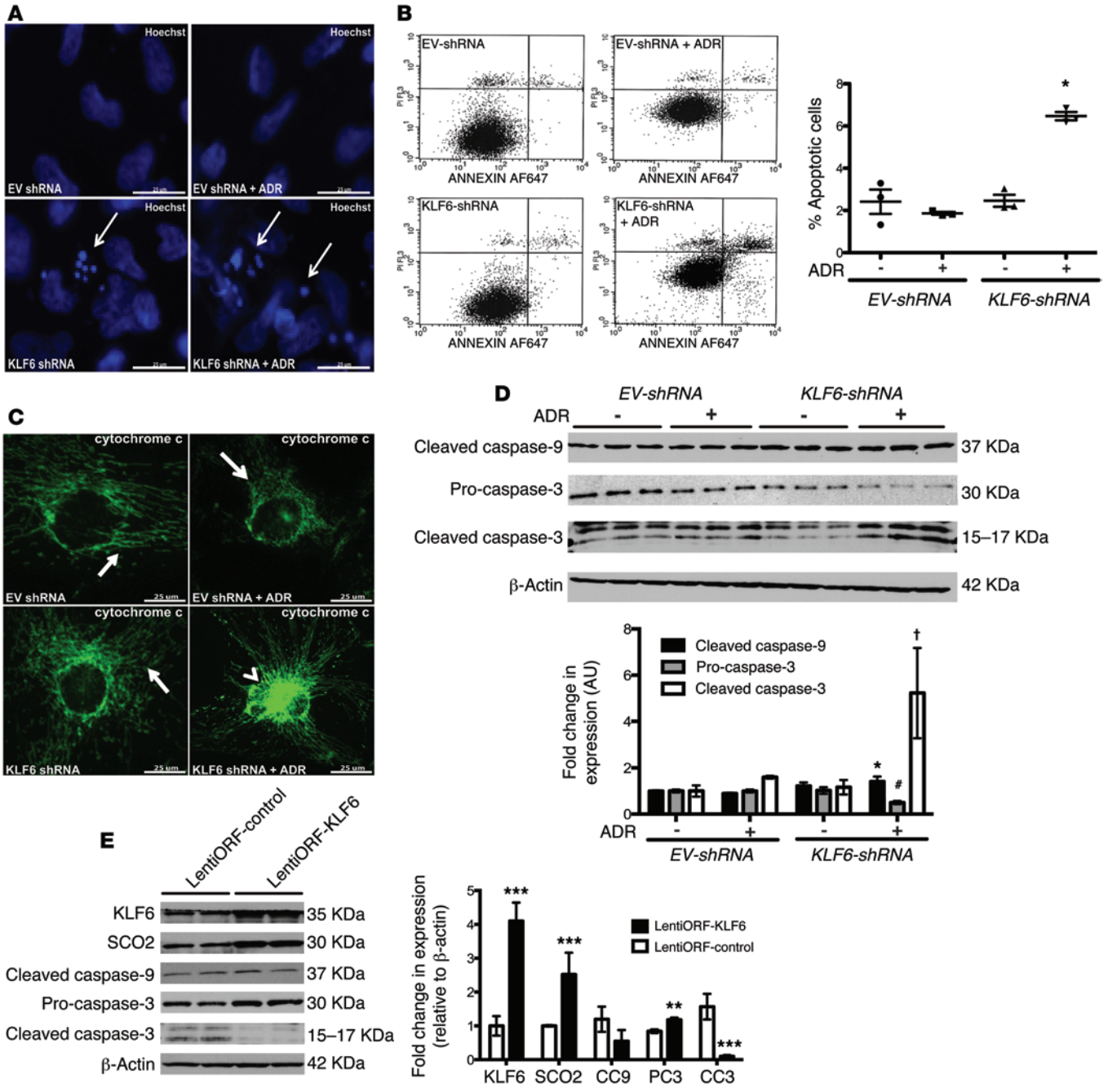

Figure 9. shRNA-mediated *KLF6* knockdown resulted in activation of the intrinsic apoptotic pathway. Cultured human podocytes (*EV-shRNA* and *KLF6-shRNA*) were treated with and without ADR for 24 hours. (**A**) Immunofluorescence images using Hoechst staining was performed to assess for apoptotic bodies. Representative images of six independent experiments are shown (original magnification, ×20). Arrows show apoptotic bodies. (**B**) To quantify apoptosis, annexin V/propidium iodide staining in combination with FACS was performed ($n = 3$). Kruskal-Wallis test with Dunn's post-hoc test, $^{*}P < 0.05$. (**C**) Immunofluorescence images of cytochrome *c* staining in *EV-shRNA* and *KLF6-shRNA* podocytes treated with and without ADR are shown. Representative images of six independent experiments are shown to demonstrate the distribution of cytochrome *c* staining (original magnification, ×20). Arrows show mitochondrial cytochrome *c* distribution. Arrowhead shows cytosolic distribution of cytochrome *c*. (**D**) Activation of the intrinsic apoptotic pathway was assessed using Western blot analysis for cleaved caspase-9, pro–caspase-3, and cleaved caspase-3 and is shown with β-actin as a loading marker. The representative images of six independent experiments are shown in the top panel. Quantification by densitometry ($n = 6$) is shown in the bottom panel. Kruskal-Wallis test with Dunn's post-hoc test, $^{*}P < 0.05$ vs. treated and untreated EV-shRNA, $^{\#}P < 0.05$ vs. all groups, $^{\dagger}P < 0.01$ vs. all groups. (**E**) To confirm whether the preservation of KLF6 prevents apoptosis, Western blot analysis was performed on human podocyte lysates from ADR-treated podocytes with (LentiORF-*KLF6*) and without (LentiORF-control) *KLF6* overexpression. Representative images of three independent experiments are shown in the top panel (cleaved caspase-3 and pro–caspase-3 are from the same samples run on parallel gels). Quantification by densitometry ($n = 3$) is shown in the bottom panel. Mann-Whitney *U* test, $^{***}P < 0.001$, $^{**}P < 0.01$.

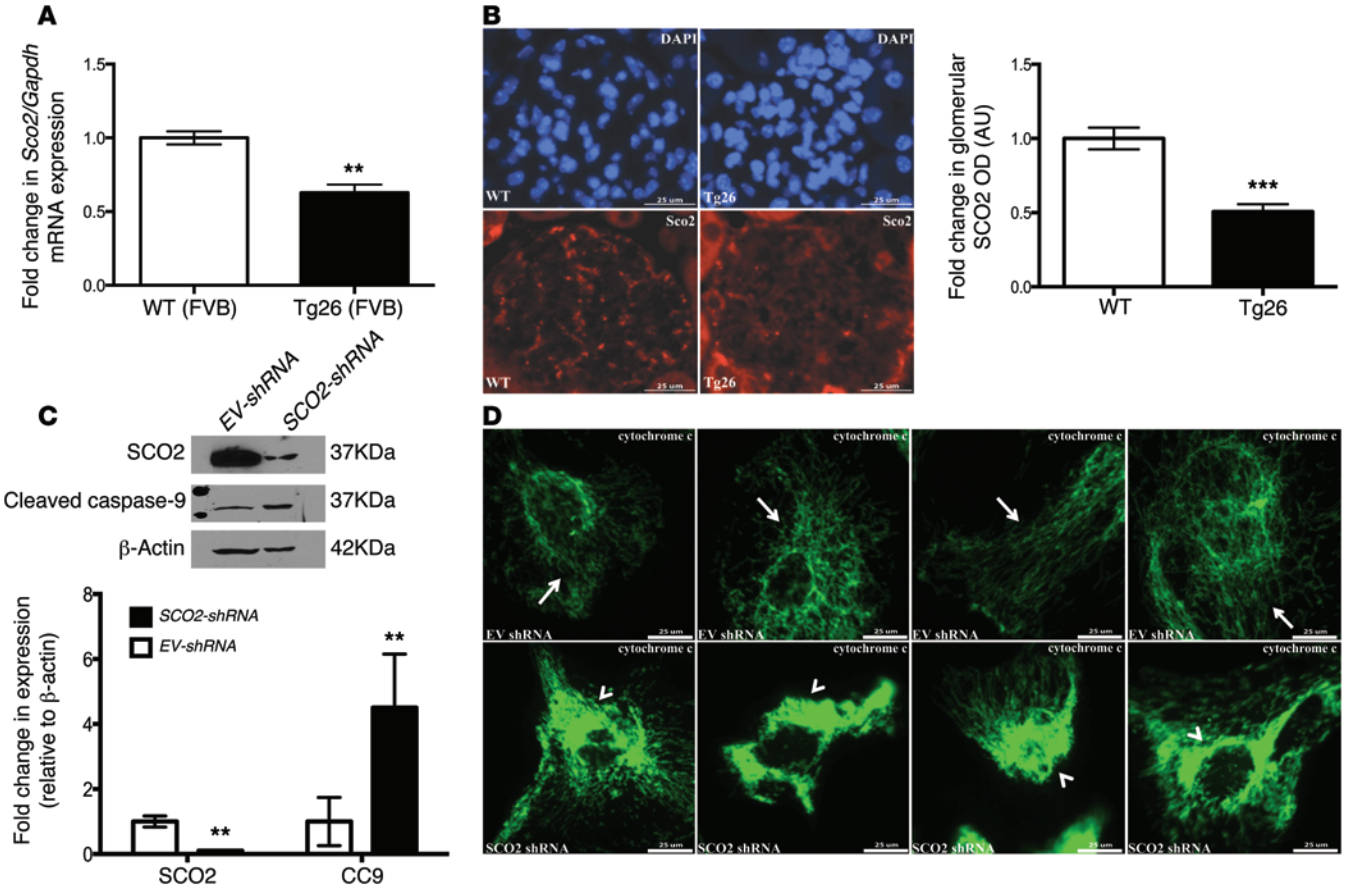

Figure 10. SCO2, a downstream target of KLF6, is critical to preventing the activation of intrinsic apoptotic pathway. Primary podocytes were isolated from WT and Tg26 mice (FVB/N). RNA was extracted, and real-time PCR was performed. (**A**) *Sco2* mRNA expression was compared between WT and Tg26 mice ($n = 5$). Mann-Whitney *U* test, $^{**}P < 0.01$. (**B**) SCO2 expression was confirmed using immunofluorescence. Representative images of six independent experiments are shown in the left panel (original magnification, ×20). A total of 30 glomeruli per mouse were selected, and SCO2 expression was quantified in the glomerular region ($n = 6$) as shown in the right panel. Unpaired *t* test $^{***}P < 0.001$. (**C**) To assess the role of SCO2 in mitochondrial injury, shRNA-mediated *SCO2* knockdown was performed in human podocytes. Western blot analysis was performed for SCO2 and cleaved caspase-9. Representative blots from three independent experiments are shown in the top panel. Quantification by densitometry ($n = 3$) is shown in the bottom panel. Mann-Whitney *U* test, $^{**}P < 0.01$. (**D**) Immunofluorescence images of cytochrome *c* staining in *EV-shRNA* and *SCO2-shRNA* podocytes are shown. Representative images of four independent experiments are shown to demonstrate the distribution of cytochrome *c* staining (original magnification, ×20). Arrows show mitochondrial cytochrome *c* distribution. Arrowheads show cytosolic distribution of cytochrome *c*.

the podocin promoter (B6.Cg-Tg [NPHS2-cre] 295Lbh/J; Jackson Laboratory). After backcrossing, male offspring expressing *Cre* with two floxed *Klf6* alleles were used as the experimental group (*Podocin-Cre Klf6*$^{fl/fl}$). Mice with two WT alleles and *Cre* expression were used as controls (*Podocin-Cre Klf6*$^{+/+}$). Genotyping by tail preparation and PCR were performed at 2 weeks of age as previously described (35).

ADR murine model. In the ADR model, *Podocin-Cre Klf6*$^{fl/fl}$ and *Podocin-Cre Klf6*$^{+/+}$ mice (12 weeks of age) were administered ADR (18 mg/kg) intravenously by tail vein injection (10). Urine was collected weekly to assess for albuminuria, and mice were sacrificed 5 weeks after treatment. As demonstrated by previous studies (36), at 2 weeks after ADR treatment, there is typically glomerular hypertrophy with hyaline droplets. At 4 weeks after ADR treatment, there is typically mesangial expansion, tubular vacuolization, and mild interstitial proliferation. Significant glomerulosclerosis and tubulointerstitial inflammation were not observed until week 6. Since our study was performed on a resistant mouse strain (C57BL/6) and we observed a significant increase in albuminuria at 5 weeks, we sacrificed the mice at this time point to determine the extent of glomerular injury and tubulointerstitial injury.

Measurement of urine albumin and creatinine. Urine albumin was quantified by ELISA using a kit from Bethyl Laboratory Inc. Urine creatinine levels were measured in the same samples using the QuantiChrom Creatinine Assay Kit (DICT-500) (BioAssay Systems) according to the manufacturer's instructions. The urine albumin excretion rate was expressed as the ratio of albumin to creatinine.

Isolation of glomeruli from mice for RNA extraction. Mouse glomeruli were isolated as previously described (37). Briefly, mice were perfused with HBSS containing 2.5 mg/ml iron oxide and 1% bovine serum albumin. At the end of perfusion, the kidneys were removed, decapsulated, minced into 1-mm^3 pieces, and digested in HBSS containing 1 mg/ml collagenase A and 100 U/ml deoxyribonuclease I. Digested tissue was then passed through a 100-micron cell strainer and collected by centrifugation. The pellet was resuspended in 2 ml HBSS, and glomeruli were collected using a magnet. The purity of

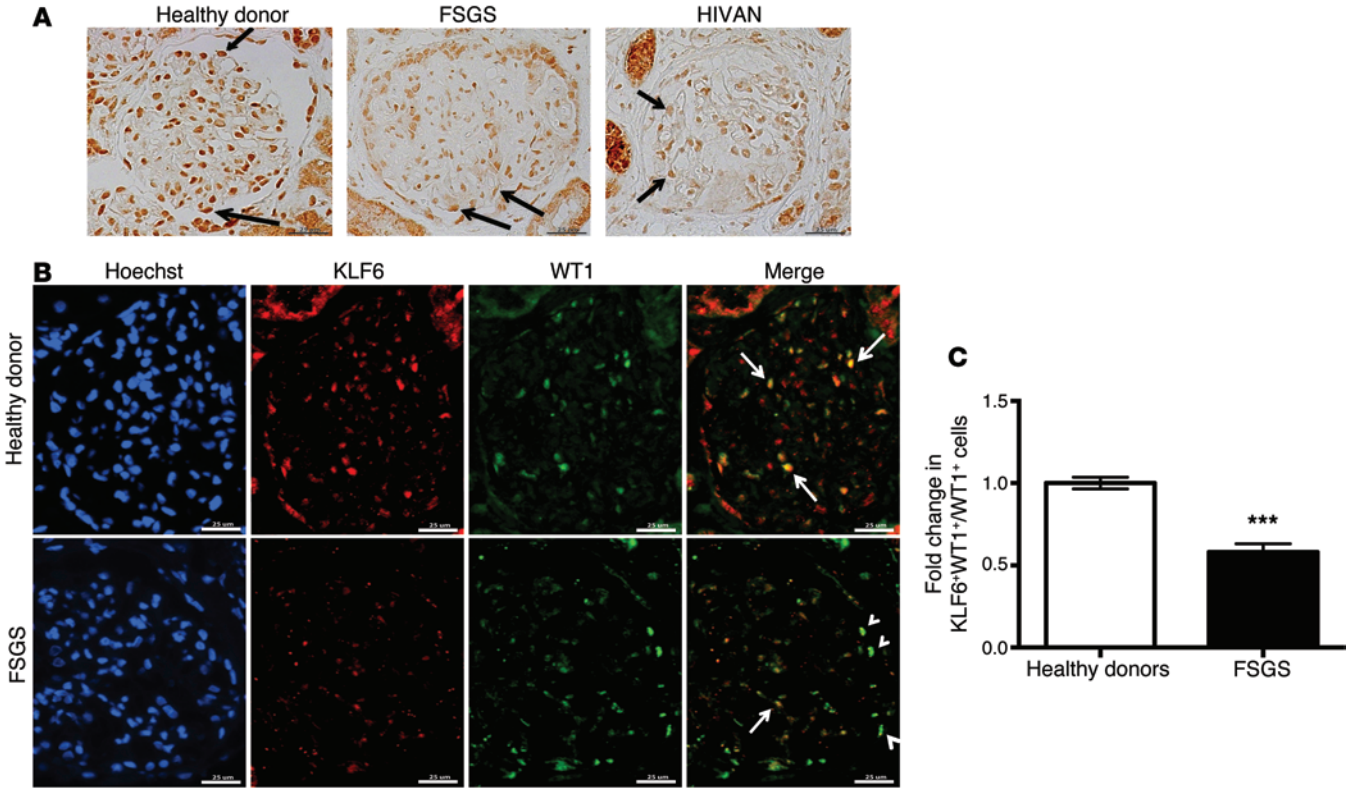

Figure 11. Reduced KLF6 expression in human HIVAN and FSGS. (**A**) Immunostaining for KLF6 performed on healthy donor nephrectomy specimens shows a nuclear distribution in podocytes and parietal cells, with a nuclear and cytosolic distribution in tubular cells. By immunohistochemistry, KLF6 expression in the podocytes (arrows) is shown in the biopsy specimens from healthy donors and in patients with diagnosed HIVAN and idiopathic noncollapsing FSGS. Representative images of six subjects in each group are shown (original magnification, ×20). (**B**) Immunofluorescence was performed using WT1 (podocyte-specific marker) to colocalize for podocyte-specific KLF6 expression in renal biopsy specimens from 10 healthy donor nephrectomies and in 10 patients with idiopathic noncollapsing FSGS. Representative images from 10 subjects in each group are shown (original magnification, ×20). Arrows show colocalization of KLF6 to WT1. Arrowheads show a lack of colocalization of KLF6 to WT1. (**C**) Twenty glomeruli per biopsy specimen were selected, and quantification of KLF6 staining in the podocytes was determined as the ratio of $KLF6^+WT1^+$ cells to $WT1^+$ cells (n = 10). Mann-Whitney U test, $^{***}P < 0.001$.

glomeruli was verified by microscopy. Total RNA was isolated from the kidney glomeruli of mice using TRIzol (Life Technologies).

Isolation of primary mouse podocytes. After glomerular isolation, primary mouse podocytes were isolated as previously described (38). In brief, isolated glomeruli were initially cultured on collagen I–coated culture dishes in RPMI 1640 medium containing 10% fetal bovine serum (Cansera International) supplemented with 1% Insulin-Transferrin-Selenium-A liquid media supplement (Life Technologies) and 100 U/ml penicillin. Cultures were incubated at 37°C in a humidified incubator. Subculture of primary podocytes was performed after 5 days of culture of isolated glomeruli. Cellular outgrowths were detached with Trypsin–EDTA (Sigma-Aldrich) and passed through a 40-μm sieve to remove the remaining glomerular cores. The filtered cells were cultured on collagen I–coated dishes and processed for RNA or protein preparation.

Cell culture. Conditionally immortalized murine and human podocytes were gifts from Peter Mundel (Massachusetts General Hospital, Boston, Massachusetts, USA) and Moin Saleem (University of Bristol, Southmead Hospital, Bristol, United Kingdom). Methods for podocyte cultivation, immortalization, and differentiation were based on a previously described protocol (29). These cells proliferate under permissive conditions (gamma interferon at 33°C), but differentiate under nonpermissive conditions (37°C).

Infection of human podocytes with HIV-1 or control vector. HIV constructs have been described previously (39). Briefly, HIV-1 gag/pol-deleted construct pNL4-3:d1443 was derived from the provirus pNL4-3. A fragment that contained the *EGFP* gene (from pEGFP-C1; Clontech Laboratories Inc.) was inserted at the SphI/MscI gag/pol deletion site. The HIV-1 gag/pol genes and the VSV-G envelope glycoprotein were provided in *trans* using pCMV R8.91 and pMD.G plasmids, respectively (gifts from Didier Trono, Salk Institute, La Jolla, California, USA). As a negative control, the virus was also produced from pHR-CMV-IRES2-GFP-ΔB, which contains the HIV-1 long-term repeat and EGFP. In all experiments, cells were grown at 37°C on type I collagen–coated dishes for 10 days to inactivate the temperature-sensitive T antigen and to allow for differentiation.

shRNA-mediated KLF6 knockdown using lentivirus. *KLF6* knockdown in human podocytes was performed using an Expression Arrest GIPZ Lentiviral shRNAmir system (Thermo Scientific). Lentiviral particles were produced by transfecting 293T cells with a combination of lentiviral expression plasmid DNA, pCD/NL-BH ΔΔΔ packaging plasmid, and VSV-G–encoding pLTR-G plasmid. For cell infection, viral supernatants were supplemented with 8 μg/ml polybrene and incubated with cells for a 24-hour period. Cells expressing shRNA were selected with puromycin for 2 to 3 weeks prior to use in all studies. GFP expression and Western blot analysis were performed to confirm *KLF6* knockdown.

shRNA-mediated SCO2 knockdown. *SCO2* shRNA clone was purchased from Thermo Scientific, and shRNA-mediated *SCO2* knockdown was achieved by transfecting human podocytes using Lipofectamine 3000 (Life Technologies). Cells expressing shRNA were selected with puromycin for 3 days prior to use in all studies. GFP expression and Western blot analysis were performed to confirm *SCO2* knockdown.

LentiORF-KLF6 overexpression. LentiORF-*KLF6* clone was purchased from Thermo Scientific, and transient KLF6 overexpression was achieved by transfecting human podocytes using Lipofectamine 3000 (Life Technologies). Cells expressing GFP were selected with blasticidin for 3 days prior to use in all studies. GFP expression and Western blot analysis were performed to confirm *KLF6* overexpression.

ADR treatment of podocytes in culture. Human podocytes were differentiated for 14 days at 37°C prior to all experiments. Human podocytes were treated with 0.4 μg/ml ADR (Sigma-Aldrich) or a control vehicle for a period of 6–24 hours, at 6 hour intervals, as previously described (40).

Real-time PCR. Total RNA was extracted by using TRIzol (GIBCO Life Technology). First-strand cDNA was prepared from total RNA (1.5 μg) using the SuperScript III First-Strand Synthesis Kit (Life Technologies), and cDNA (1 μl) was amplified in triplicate using SYBR GreenER qPCR Supermix on an ABI PRISM 7900HT (Applied Biosystems). Primers for human *KLF5* (SABiosciences) human *KLF4*, *KLF6*, *KLF7*, *KLF8*, *KLF9*, *KLF10*, *KLF11*, *KLF12*, *KLF13*, *KLF14*, *KLF15*, and *KLF16*, mouse *Klf6*, mouse *Nephrin*, mouse *Podocin*, mouse *Nrf1*, mouse *Polrmt*, mouse *Tfam*, mouse *mt-Co2* (mitochondrial encoded), mouse *Cox8a*, mouse *Mpv17*, and mouse *Sco2* were designed using NCBI/Primer-BLAST and were validated for efficiency prior to application (Supplemental Table 1). Light cycler analysis software was used to determine crossing points using the second derivative method. Data were normalized to housekeeping genes (*GAPDH*) and presented as fold increase compared with RNA isolated from the control group using the $2^{-\Delta\Delta CT}$ method.

Promoter analysis. Using TRANSFAC software (BIOBASE Biological Databases) (15), we scanned the promoters of all mouse genes in the region from −2,000 to +500 of the transcription start site with the KLF6 position weight matrix provided by the TRANSFAC system. Total counts for KLF6 binding sites for each gene were accumulated in a table and sorted by the number of identified sites.

ChIP. Prior to performing the ChIP, KLF6 was overexpressed in HEK 293 cells using the Precision LentiORF pLOC lentiviral vectors (Open Biosystems). HEK 293 cells were acquired from ATCC (catalog #CRL-1573). These are lentivirus-based vectors in which the open reading frame (ORF) for *KLF6* has been cloned downstream of the CMV promoter and contain GFP as a reporter gene. A scrambled LentiORF-control was used as a negative control. HEK 293 cells were transfected with Lipofectamine 3000 (Life Technologies).

The ChIP assay was performed using a kit from Cell Signaling Technology according to the manufacturer's protocol. Briefly, 3×10^7 cultured HEK 293 cells were cross-linked with formaldehyde for 10 minutes, followed by the addition of 1:20 volume of 2.5 M glycine to quench unreacted formaldehyde. Cells were lysed using a series of non-SDS-containing buffers according to the manufacturer's protocol. Chromatin extracted from the lysed cells was sonicated using a Misonix Sonicator 3000 with Microtip to generate chromatin fragments of between 300 and 1,000 bp. Immunoprecipitation of KLF6-cross-linked chromatin was carried out using Dynabeads M-280 (Cell Signaling Technology) preincubated with rabbit anti-KLF6 (SC-7158; Santa Cruz Biotechnology Inc.) antibody. To control for nonspecific IgG binding, rabbit IgG (Cell Signaling Technology Inc.) was used. After incubation of chromatin with antibody-coupled Dynabeads, the beads were washed several times, and immunoprecipitated chromatin complexes were eluted from the beads. DNA-protein cross-links were reversed by incubation at 65°C for 6 hours, and then RNase A and proteinase K were added sequentially to remove RNA and proteins. Purified DNA was used for the analysis of the *SCO2* proximal promoter region (−2 kb) by real-time PCR on an ABI PRISM 7900HT (Life Technologies) using SYBR GreenER qPCR Supermix. PCR primers for human *SCO2* promoter region were derived from an available sequence (GenBank accession no. CAG30455.1), and the primers were designed using SABiosciences GPH1022775(–)02A and GPH1022775(+)01A. The relative amplification of the promoter sequence of each gene was calculated using the $2^{-\Delta\Delta CT}$ method, and normalization was performed against the 1:100 diluted input of DNA.

Western blot analysis. Glomeruli were lysed with a buffer containing 1% Triton, a protease inhibitor cocktail, and tyrosine and serine-threonine phosphorylation inhibitors. Lysates were subjected to immunoblot analysis using rabbit anti-KLF6 (SC-7158; Santa Cruz Biotechnology Inc.), rabbit anti–β-actin (A1978; Sigma-Aldrich), rabbit anti-GAPDH (MAB374; Millipore), and rabbit anti–cleaved caspase-3 (9664S; Cell Signaling Technology).

Mitochondrial fragmentation studies. To visualize mitochondrial morphology, differentiated human podocytes were incubated with rosamine-based MitoTracker probe (Life Technologies) at 100 nM for 30 minutes. After the incubation period, cells were washed with PBS and fixed with 3.7% formaldehyde in growth medium. Mitochondrial fragmentation was quantified using a previously described method (41). Briefly, mitochondrial morphology was categorized in each cell, by an investigator blinded to the experimental protocol, as tubular (>75% of mitochondria with tubular length >5 mm), intermediate (25%–75% of mitochondria with tubular length >5 mm), or fragmented (<25% of mitochondria with tubular length >5 mm).

Immunocytochemistry. Differentiated human podocytes were initially washed with PBS and subsequently fixed with 3.7% formaldehyde in growth medium. Cells were washed and permeabilized with 0.25% Triton X-100. Cells were blocked in 10% normal horse serum and incubated with primary antibody overnight (mouse anti-KLF6 [SC-365633; Santa Cruz Biotechnology Inc.]), rabbit anti–cleaved caspase-3 [9664S; Cell Signaling Technology], and mouse anti–cytochrome *c* [556432; BD Pharmingen]). On the next day, the cells were washed with PBS and incubated in secondary antibody in 10% normal horse serum (NHS). Subsequently, the cells were washed and incubated with Hoechst (Ana Spec Inc.) prior to mounting.

ATP quantification assay. ATP levels were determined in differentiated human podocytes with and without ADR treatment using a luciferase-based ATP Determination Kit (Life Technologies) according to the manufacturer's protocol. Briefly, differentiated human podocytes were grown in a 24-well plate. Cells were initially washed and subsequently treated with ATP-releasing agent (Sigma-Aldrich). There were 10 μl of cells in the ATP-releasing agent used to determine ATP levels, and the remainder was used to quantify protein levels using a Pierce BCA Protein Assay Kit (Thermo Scientific) with BSA as a standard.

Mitochondrial membrane potential. Mitochondrial membrane potential was determined using MitoProbe $DiIC_1(5)$ Assay Kit according to the manufacturer's protocol (Life Technologies). Human podocytes with and without *KLF6* knockdown were initially labeled with $DiIC_1(5)$ for 15 minutes at 37°C. Subsequently, the cells were washed and analyzed using a flow cytometer with 633 nm excitation. Mitochondrial membrane potential was defined as the change in $DiIC_1(5)$ fluorescence. Carbonyl cyanide 3-chlorophenylhydrazone (CCCP) served as the positive control.

Mitochondrial biomass. Mitochondrial biomass was measured as previously described (42). Briefly, human podocytes treated with and without ADR were stained with the MitoTracker Deep Red FM dye (Life Technologies) to measure mitochondrial mass independent of membrane potential. Subsequently, the cells were washed and analyzed using a flow cytometer with 644 nm excitation.

Oxygen consumption rate. An assay using the phosphorescent oxygen-sensing probe MitoXpress (Cayman Chemical) was performed to measure extracellular oxygen consumption as previously described (43). Briefly, human podocytes were initially treated with serum-free medium containing either control vehicle or ADR. Mineral oil was used to prevent the loss of extracellular oxygen. Subsequently, fluorescence was measured with 380 nm excitation every 3 minutes over a 3-hour period. The slope of the curve represented the rate of oxygen consumption (μs/h). The relative change in oxygen consumption rate (OCR) as compared with untreated *EV-shRNA* human podocytes was presented.

Annexin V/propidium iodide assay for apoptosis. Differentiated human podocytes treated with and without ADR were evaluated for apoptosis using the Annexin V conjugate (Alexa Fluor 647, Life Technologies) and propidium iodide (PI) (BD Pharmingen) according to the manufacturer's protocol. Stained cells were assessed for apoptotic activity using a FACSCalibur flow cytometer at Stony Brook Medicine with data analysis of 10,000 gated events. Apoptotic cells were defined as cells with low PI and high annexin binding.

Histopathology by bright-field light microscopy. Mice were perfused with HBSS, and the kidneys were fixed in 10% phosphate buffered formalin overnight and switched to 70% ethanol prior to processing for histology. Kidney tissue was embedded in paraffin by American Histolabs, and 3-μm-thick sections were stained with periodic acid–Schiff (PAS) (Sigma-Aldrich).

Histopathology by transmission electron microscopy. Mice were perfused with PBS and then immediately fixed in 2.5% glutaraldehyde for electron microscopy as previously described (44). After embedding of kidney tissues in epoxy resin, ultrathin sections were stained with uranyl acetate and lead citrate, mounted on a copper grid, and photographed under a Hitachi H7650 microscope. Briefly, negatives were digitized, and images with a final magnification of approximately ×3,000, ×10,000, ×50,000, and ×75,000 were obtained. Quantification of dysmorphic mitochondria was performed as previously described (45, 46). Briefly, a total of 100 mitochondria in the podocytes from all groups were initially identified. Dysmorphic mitochondria were defined as mitochondria with a focal loss of visible cristae (45), clustering of residual cristae at the peripheral mitochondrial membrane (45), and fragmented (<2 μm in length) (46).

Immunohistochemistry. Archival human biopsy specimens of healthy donor nephrectomies, HIVAN, and idiopathic FSGS for IHC were collected at Stony Brook University School of Medicine and Mount Sinai School of Medicine under a protocol approved by its Institutional Review Board. Specimens were initially baked for 20 minutes at 55–60°C and were then processed as previously described (9). Briefly formalin-fixed and paraffin-embedded sections were deparaffinized, and endogenous peroxidase was inactivated with H_2O_2. Sections were then blocked in 2% goat serum in PBS for 1 hour at room temperature and were then incubated with an anti–rabbit KLF6 antibody (SC-7158; Santa Cruz Biotechnology Inc.) at 4°C overnight. The next day, sections were washed three times with PBS and then incubated with secondary antibody for 30 minutes. Positive staining was revealed by peroxidase-labeled streptavidin and diaminobenzidine substrate. The control included a section stained with only secondary antibody.

Immunofluorescence. Kidney sections from these mice were prepared in identical fashion. Immunostaining was performed using rabbit anti-KLF6 (SC-7158; Santa Cruz Biotechnology Inc.) and mouse anti-WT1 antibodies (SC-7385; Santa Cruz Biotechnology Inc.). After washing, sections were incubated with a fluorophore-linked secondary antibody (Alexa Fluor 488–anti-rabbit IgG and Alexa Fluor 568–anti-mouse IgG; A10468, A10494; Life Technologies). After staining, slides were mounted in Aqua Poly/Mount (Polysciences Inc.) and photographed under an AxioVision IIe microscope with a digital camera. KLF6 staining in the podocytes was quantified as the ratio of $KLF6^+WT1^+$ cells to $WT1^+$ cells using ImageJ 1.26t software (NIH ImageJ; http://rsb.info.nih.gov/ij/). Using a similar strategy, immunostaining for SCO2 and staining for MT-CO2 and podocalyxin were performed using mouse anti–MT-CO2 (MitoSciences, MS405) and mouse anti-podocalyxin antibodies (AF1556; R&D Biosystems).

Statistics. Unpaired two-tailed *t* test was used to compare data between two groups and two-way ANOVA with Tukey's post-hoc test to compare data between more than two groups. Since we could not assume normality on some of the other data sets with smaller sample sizes, nonparametric statistical tests were performed using the Mann-Whitney *U* test to compare data between the two groups and the Kruskal-Wallis test with Dunn's post-hoc test to compare data between more than two groups. The exact test used for each experiment is noted in the figure legends. Data are expressed as mean ± SEM (X ± SEM). All experiments were repeated a minimum of three times, and representative experiments are shown. Statistical significance was considered when $P < 0.05$. All statistical analysis was performed using GraphPad Prism 5.0a.

Study approval. The Mount Sinai School of Medicine Animal Institute Committee approved all animal studies, and the NIH *Guide for the Care and Use of Laboratory Animals* was followed strictly. The Stony Brook University Institutional Review Board approved the use of archived, de-identified human biopsy specimens for immunostaining.

Acknowledgments

This work was supported by NIH/NIDDK 1 R01 DK078897-01 and Chinese 973 fund 2012CB517601 to J.C. He; and NIH/NIDDK 1K0801DK102519-01 and Dialysis Clinic Inc. (Paul Teschan Research Grant) to S.K. Mallipattu. We thank Ali Gharavi, Natalia Papeta, and Roel Sterken (Division of Nephrology, Department of Medicine, Columbia University, New York, New York, USA) for their guidance and constructive feedback on the data presented in this article.

Address correspondence to: John Cijiang He, Department of Medicine/Nephrology, Mount Sinai School of Medicine, One Gustave L. Levy Place, Box 1243m, New York, New York 10029, USA. Phone: 212.659.1703; E-mail: cijiang.he@mssm.edu. Or to: Sandeep K. Mallipattu, Department of Medicine/Nephrology, Stony Brook University, 100 Nicolls Road, HSCT17-090B, Stony Brook, New York 11790, USA. Phone: 631.638.2164; E-mail: sandeep.mallipattu@stonybrookmedicine.edu.

1. Meyrier A. Mechanisms of disease: focal segmental glomerulosclerosis. *Nat Clin Pract Nephrol*. 2005;1(1):44–54.
2. Wiggins RC. The spectrum of podocytopathies: a unifying view of glomerular diseases. *Kidney Int*. 2007;71(12):1205–1214.
3. Holthofer H, et al. Altered gene expression and functions of mitochondria in human nephrotic syndrome. *FASEB J*. 1999;13(3):523–532.
4. Solin ML, Pitkanen S, Taanman JW, Holthofer H. Mitochondrial dysfunction in congenital nephrotic syndrome. *Lab Invest*. 2000;80(8):1227–1232.
5. Barisoni L, et al. Collapsing glomerulopathy associated with inherited mitochondrial injury. *Kidney Int*. 2008;74(2):237–243.
6. Papeta N, et al. Prkdc participates in mitochondrial genome maintenance and prevents Adriamycin-induced nephropathy in mice. *J Clin Invest*. 2010;120(11):4055–4064.
7. McConnell BB, Yang VW. Mammalian Kruppel-like factors in health and diseases. *Physiol Rev*. 2010;90(4):1337–1381.
8. Cohen CD, et al. Comparative promoter analysis allows de novo identification of specialized cell junction-associated proteins. *Proc Natl Acad Sci U S A*. 2006;103(15):5682–5687.
9. Mallipattu SK, et al. Kruppel-Like factor 15 (KLF15) is a key regulator of podocyte differentiation. *J Biol Chem*. 2012;287(23):19122–19135.
10. Lee VW, Harris DC. Adriamycin nephropathy: a model of focal segmental glomerulosclerosis. *Nephrology*. 2011;16(1):30–38.
11. Tewey KM, Rowe TC, Yang L, Halligan BD, Liu LF. Adriamycin-induced DNA damage mediated by mammalian DNA topoisomerase II. *Science*. 1984;226(4673):466–468.
12. Adachi K, et al. A deletion of mitochondrial DNA in murine doxorubicin-induced cardiotoxicity. *Biochem Biophys Res Commun*. 1993;195(2):945–951.
13. Lebrecht D, Kokkori A, Ketelsen UP, Setzer B, Walker UA. Tissue-specific mtDNA lesions and radical-associated mitochondrial dysfunction in human hearts exposed to doxorubicin. *J Pathol*. 2005;207(4):436–444.
14. Suliman HB, Carraway MS, Ali AS, Reynolds CM, Welty-Wolf KE, Piantadosi CA. The CO/HO system reverses inhibition of mitochondrial biogenesis and prevents murine doxorubicin cardiomyopathy. *J Clin Invest*. 2007;117(12):3730–3741.
15. Matys V, et al. TRANSFAC: transcriptional regulation, from patterns to profiles. *Nucleic Acids Res*. 2003;31(1):374–378.
16. Pecina P, Houstkova H, Hansikova H, Zeman J, Houstek J. Genetic defects of cytochrome c oxidase assembly. *Physiol Res*. 2004; 53(suppl 1):S213–S223.
17. Banci L, et al. A structural characterization of human SCO2. *Structure*. 2007;15(9):1132–1140.
18. Arola OJ, Saraste A, Pulkki K, Kallajoki M, Parvinen M, Voipio-Pulkki LM. Acute doxorubicin cardiotoxicity involves cardiomyocyte apoptosis. *Cancer Res*. 2000;60(7):1789–1792.
19. Liu TJ, et al. Ginkgo biloba extract 761 reduces doxorubicin-induced apoptotic damage in rat hearts and neonatal cardiomyocytes. *Cardiovasc Res*. 2008;80(2):227–235.
20. Yeh YC, et al. A standardized extract of Ginkgo biloba suppresses doxorubicin-induced oxidative stress and p53-mediated mitochondrial apoptosis in rat testes. *Br J Pharmacol*. 2009;156(1):48–61.
21. Mallipattu SK, et al. Expression of HIV transgene aggravates kidney injury in diabetic mice. *Kidney Int*. 2013;83(4):626–634.
22. Zhang R, Han M, Zheng B, Li YJ, Shu YN, Wen JK. Kruppel-like factor 4 interacts with p300 to activate mitofusin 2 gene expression induced by all-trans retinoic acid in VSMCs. *Acta Pharmacol Sin*. 2010;31(10):1293–1302.
23. Johar K, Priya A, Dhar S, Liu Q, Wong-Riley MT. Neuron-specific specificity protein 4 bigenomically regulates the transcription of all mitochondria- and nucleus-encoded cytochrome c oxidase subunit genes in neurons. *J Neurochem*. 2013;127(4):496–508.
24. Ross MJ, Martinka S, D'Agati VD, Bruggeman LA. NF-κB regulates Fas-mediated apoptosis in HIV-associated nephropathy. *J Am Soc Nephrol*. 2005;16(8):2403–2411.
25. Chuang PY, Yu Q, Fang W, Uribarri J, He JC. Advanced glycation endproducts induce podocyte apoptosis by activation of the FOXO4 transcription factor. *Kidney Int*. 2007;72(8):965–976.
26. Papadopoulou LC, et al. Fatal infantile cardioencephalomyopathy with COX deficiency and mutations in SCO2, a COX assembly gene. *Nat Genet*. 1999;23(3):333–337.
27. Jaksch M, et al. Mutations in SCO2 are associated with a distinct form of hypertrophic cardiomyopathy and cytochrome c oxidase deficiency. *Hum Mol Genet*. 2000;9(5):795–801.
28. He JC, et al. Nef stimulates proliferation of glomerular podocytes through activation of Src-dependent Stat3 and MAPK1,2 pathways. *J Clin Invest*. 2004;114(5):643–651.
29. He JC, et al. Retinoic acid inhibits HIV-1-induced podocyte proliferation through the cAMP pathway. *J Am Soc Nephrol*. 2007;18(1):93–102.
30. Smeets B, et al. Parietal epithelial cells participate in the formation of sclerotic lesions in focal segmental glomerulosclerosis. *J Am Soc Nephrol*. 2011;22(7):1262–1274.
31. Husain M, et al. Inhibition of p66ShcA longevity gene rescues podocytes from HIV-1-induced oxidative stress and apoptosis. *J Biol Chem*. 2009;284(24):16648–16658.
32. Snyder A, et al. FAT10: a novel mediator of Vpr-induced apoptosis in human immunodeficiency virus-associated nephropathy. *J Virol*. 2009;83(22):11983–11988.
33. Dickie P, et al. HIV-associated nephropathy in transgenic mice expressing HIV-1 genes. *Virology*. 1991;185(1):109–119.
34. Feng X, et al. Reduction of Stat3 activity attenuates HIV-induced kidney injury. *J Am Soc Nephrol*. 2009;20(10):2138–2146.
35. Leow CC, et al. Prostate-specific Klf6 inactivation impairs anterior prostate branching morphogenesis through increased activation of the Shh pathway. *J Biol Chem*. 2009;284(31):21057–21065.
36. Lee TI, Johnstone SE, Young RA. Chromatin immunoprecipitation and microarray-based analysis of protein location. *Nat Protoc*. 2006;1(2):729–748.
37. Takemoto M, et al. A new method for large scale isolation of kidney glomeruli from mice. *Am J Pathol*. 2002;161(3):799–805.
38. Katsuya K, Yaoita E, Yoshida Y, Yamamoto Y, Yamamoto T. An improved method for primary culture of rat podocytes. *Kidney Int*. 2006;69(11):2101–2106.
39. Husain M, et al. HIV-1 Nef induces proliferation and anchorage-independent growth in podocytes. *J Am Soc Nephrol*. 2002;13(7):1806–1815.
40. Guo J, et al. RAGE mediates podocyte injury in adriamycin-induced glomerulosclerosis. *J Am Soc Nephrol*. 2008;19(5):961–972.
41. Huang H, et al. piRNA-associated germline nuage formation and spermatogenesis require MitoPLD profusogenic mitochondrial-surface lipid signaling. *Dev Cell*. 2011;20(3):376–387.
42. Favre C, Zhdanov A, Leahy M, Papkovsky D, O'Connor R. Mitochondrial pyrimidine nucleotide carrier (PNC1) regulates mitochondrial biogenesis and the invasive phenotype of cancer cells. *Oncogene*. 2010;29(27):3964–3976.
43. Zhdanov AV, Ward MW, Prehn JH, Papkovsky DB. Dynamics of intracellular oxygen in PC12 cells upon stimulation of neurotransmission. *J Biol Chem*. 2008;283(9):5650–5661.
44. Mallipattu SK, et al. Diabetic nephropathy in a nonobese mouse model of Type 2 diabetes mellitus. *Am J Physiol Renal Physiol*. 2014;306(9):F1008–F1017.
45. Herlitz LC, Mohan S, Stokes MB, Radhakrishnan J, D'Agati VD, Markowitz GS. Tenofovir nephrotoxicity: acute tubular necrosis with distinctive clinical, pathological, and mitochondrial abnormalities. *Kidney Int*. 2010;78(11):1171–1177.
46. Brooks C, Wei Q, Cho SG, Dong Z. Regulation of mitochondrial dynamics in acute kidney injury in cell culture and rodent models. *J Clin Invest*. 2009;119(5):1275–1285.